Volume 2, Issue 2, February, 2024 **ISSN (E):** 2938-3811

PREPARATION AND STUDY OF THE OPTICAL PROPERTIES OF CORE SHELL POLY 3-hexylthiophene@(SiO2 , ZnO , Ag) NPs

Ahmed Ismael
Hussein F.Hussein
Salah S. Al-luaibi*
Physics Department, College of Education for Pure Sciences, Basrah University
* Chemistry department, College of Science, Basrah University
salahshakir502@gmail.com
Husseinfalaih2020@gmail.com
ahmed.nano86@gmail.com

Abstract
The study explores enhancing the optical of core shell polymers by incorporating Poly 3-hexylthiophene@NP (SiO2, ZnO, Ag) into photo-electro-active layers useful in solar cell applications. These materials were examined and analyzed using various techniques like X-ray diffraction (XRD), scanning electron microscopy (SEM), Fourier transform infrared spectroscopy (FTIR), Atomic Force Microscopy (AFM), and UV-visible Absorption Spectrum. XRD analysis revealed high crystallinity in Poly 3-hexylthiophene @SiO2, ZnO and Ag, with crystallite sizes between 62.63 – 93.069 nm. UV-visible absorption tests indicated band gap values of 2.3 eV, 2 eV, 2.07 eV, and 2.05eV for Poly1 , Poly2 , Poly3 ,Poly4 respectively the synthesized nanoparticles.
The polymeric membrane exhibited varying thicknesses of approximately 15.4 nm, 20.6nm, 10.2 nm,
and 5.02 nm, with surface roughness values of 6.48nm, 10.4nm, 5.19nm, and 2.59 nm for Poly1 Poly2 , Poly3 ,Poly4 respectively of the polymer films. Additionally, the polymer film on the nanoparticles varied in thickness from 5.2 nm to 9.3 nm, indicating a thin, transparent layer capable of efficiently transmitting light.

Keywords: Poly 3-hexylthiophene@NPs (SiO2,ZnO,Ag),Optical properties ,Nano particles.

Introduction

Poly(3-hexylthiophene) (P3HT) is a popular material in organic optoelectronics due to its high solubility in organic solvents, making it ideal for solution processing. Additionally, P3HT has controllable crystallinity, meaning it can be manipulated and tailored for specific applications. Some applications of P3HT include solar cells, light-emitting diodes, and organic devices[1]. Considerable effort has been made to improve the intrinsic characteristics of p-type P3HT materials to enable their use in organic photovoltaic cells (OPVCs) [2].
Core-shell polymers have received great interest for future ubiquitous applications in flexible and lightweight electronic devices so they are currently being studied extensively[3 , 4]. The unique electrical and optical properties of core-shell polymers make them a great candidate to compete with the established silicon-based industry[5]. Many studies include core-shell

polymers as an active layer in organic photovoltaic cells (OSCs) [6]. Regular poly(3-hexylthiophene) (P3HT) is one of the most important and widely investigated nanopolymers (OPVCs) due to its ease of modification, better charge transfer, and self-assembly nature in solution [7, 8]. However, due to the low performance of P3HT-based devices, the marketing of P3HT-based devices has been restricted [9]. Weak crystallinity, random orientations of polymer nanochains and π-π stacking orientation of the backbone are the main concerns associated with P3HT to achieve the highest values of mobility (μ) of (OPVCs) [10,11]. In general, the core shell of Poly 3-hexylthiophene@) NPs shows the mixed structure of crystalline domains covered by amorphous domains. This superposition between domains causes changes in the charge and transfer regime between crystals [12, 13]. Therefore, there is a great need for a suitable mechanism to optimize the structural system and thus significantly improve charge transfer [14]. The one-dimensional structure of nanometer-sized polymer nanocrystals has been well proven to provide the most suitable conditions for charge transfer. This condition can be achieved through a core-shell texture of P3HT, and therefore, an efficient processing technique to decorate aligned nanocore-shell textures in a thin layer over the substrate is necessary to improve the carrier mobility [15 , 16 . 17] .

2: Materials

Various materials were sourced for this study:

- 3-hexylthiophene with a 98%+ regioregularity and a molecular weight of 168.3 g/mol from Meryer (SHANGHAI) CHEMICAL TECHNOLOGY CO., LTD.

Nanoparticles used:

- Silver Nano Particles (Ag NP) with 99.9% purity and an average size of 80nm from Hongwu International Group Ltd, China.
- Zinc Oxide Nano Particles (ZnO NP) with a size range of 20-30nm and 99.8% purity, also from Hongwu International Group Ltd.
- Silicon Dioxide Nano Particles (SiO2 NP) with 99.5% purity and an average size of 20nm from Skyspring Nanomaterials, USA**.**

All solvents utilized in this study were procured from Sigma-Aldrich.

3: Experimental

3.1: synthesis of poly (3HT)

The synthesis of 3-hexylthiophene polymer involved several sequential steps. Initially, 0.84 grams of 3-hexylthiophene were mixed with a solution comprising 50 milliliters of $CHCl_3$, and this mixture was degassed with nitrogen (N_2) for approximately 5 minutes. Subsequently, 1.62 grams of iron chloride ($FeCl_3$) were added to the degassed mixture, along with an additional 50 milliliters of $CHCl_3$, resulting in the formation of a slurry. The reaction mixture was stirred continuously for a period of 24 hours. After the stirring period, the mixture was introduced into 100 milliliters of methanol, causing the 3-hexylthiophene polymer to precipitate[18].

3.2: Core shell polymerization of P3HT@NPs(SiO_2,ZnO, Ag)

In this experiment, a core-shell polymer nanocomposite was prepared using 3-hexylthiophene and a combination of SiO_2 , ZnO , Ag nanoparticles. To initiate the synthesis, 0.84 grams of 3-hexylthiophene and an equivalent amount of the nanoparticles in a 1:4 ratio were combined. This mixture was then introduced to 50 milliliters of chloroform ($CHCl_3$) and degassed with nitrogen (N_2) for approximately 5 minutes under ultrasonic irradiation for half an hour[19]. Following degassing, 1.62 grams of ferric chloride ($FeCl_3$) and an additional 50 milliliters of $CHCl_3$ were added to create a slurry. The resulting mixture was stirred for a period of 24 hours. Subsequently, it was introduced to 100 milliliters of methanol to induce precipitation of the polymer.

4: Results and discussion

Table(1): The table represents a summary of the samples

samples	Sample summary
P3HT	Poly1
P3HT@ (25% SiO_2Np)	Poly2
P3HT @ (25% ZnO Np)	Poly3
P3HT@ (25% Ag Np)	Poly4

4.1: Fourier Transform Infrared (FT-IR) spectrums

An infrared device of Japanese origin, equipped by Shimadzu Corp. A 13750 03017, was used to determine the effective groups of the prepared polymeric membranes, as well as to determine the type of bonds that connect the atoms, whether they are weak or strong at laboratory temperature.

The FTIR analysis of Poly 3-hexylthiophene@nano SiO2, ZnO , and Ag composite material showed IN fig (1 , 2 , 3 , 4) would likely reveal distinct peaks at characteristic wavenumbers corresponding to various functional groups. For the polymer, peaks might appear at around 3050-2790 cm-1 for C-H stretching vibrations, 1600-1500 cm-1 for aromatic C=C stretching vibrations, and potentially in the region of 1000-700 cm-1 for S-containing functional groups like C-S or S-H bonds from the thiophene units[20 , 21].

In the case of SiO2, strong peaks can be anticipated at approximately 1100-1000 cm-1 for Si-O-Si stretching vibrations. Variations or shifts in these peaks when in the composite material would suggest interactions between the polymer and SiO2, manifesting as changes in peak positions or intensities[22].

Silver nanoparticles (Ag) might contribute to the spectrum with peaks around 600-400

cm-1 , potentially indicating Ag-O or Ag-C bonds. Any shifts or changes in these regions compared to the individual components would signify potential bonding or interactions between the polymer and the respective nanoparticles[23 , 24]

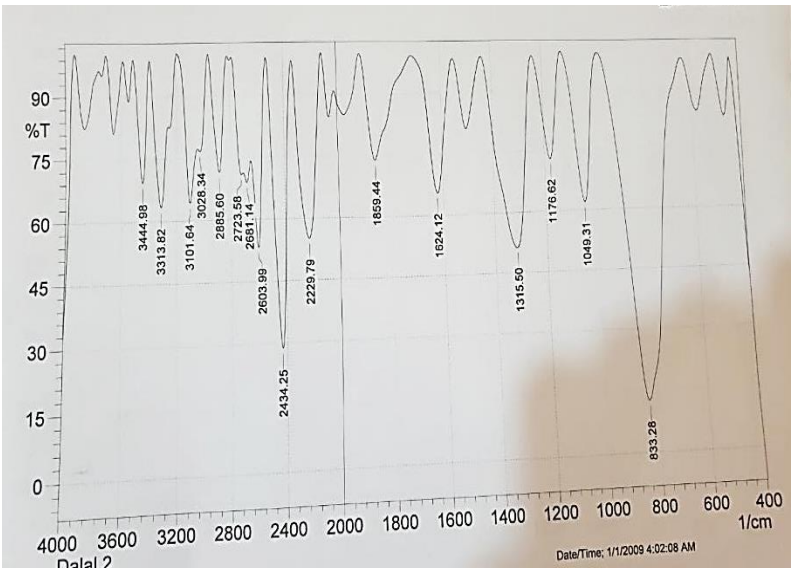

Figure (1) FT-IR Spectroscopy of Poly1

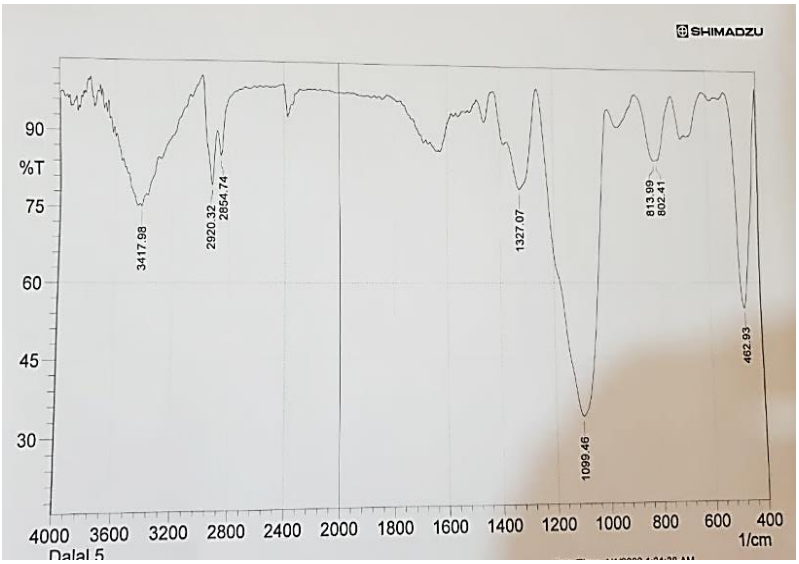

Figure (2) FT-IR Spectroscopy of Poly2

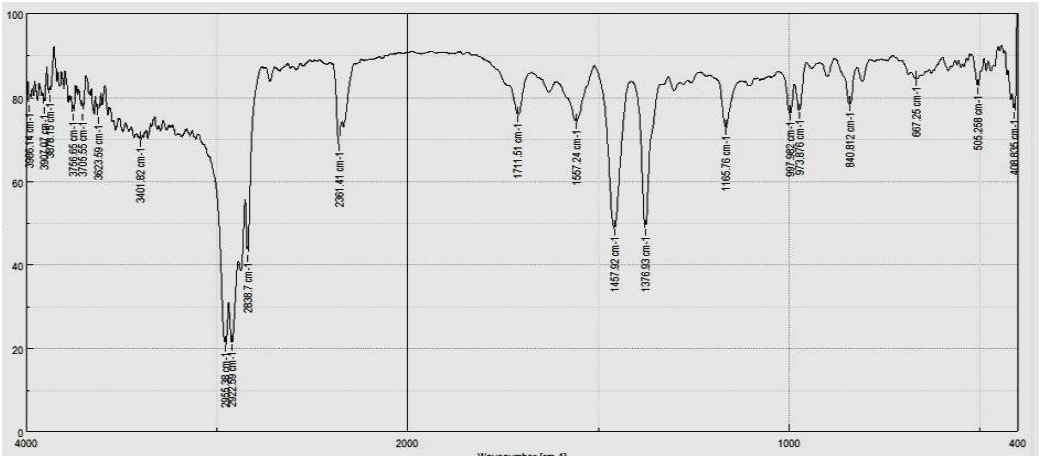

Figure (3) FT-IR Spectroscopy of Poly3

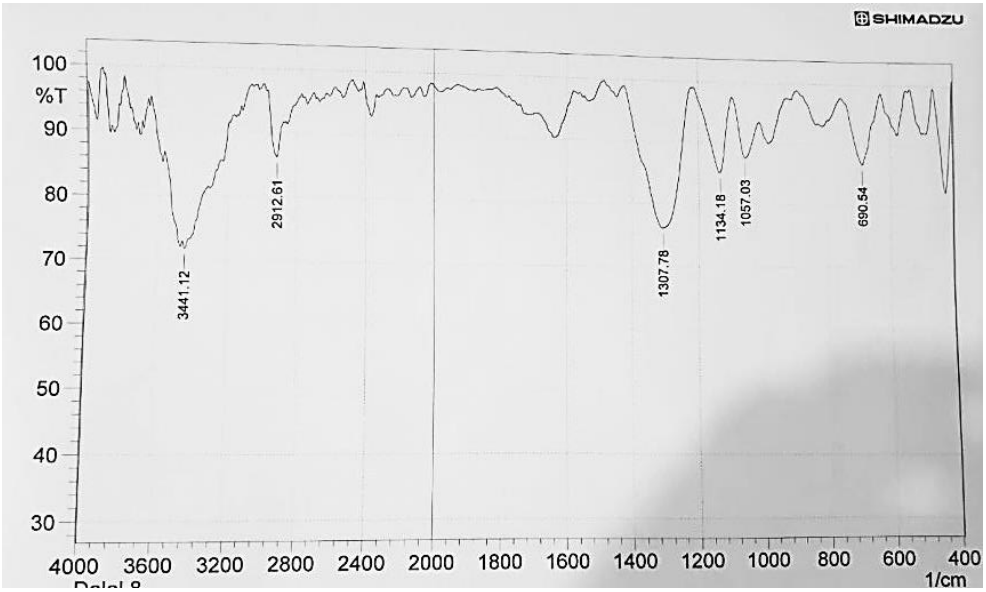

Figure (4) FT-IR Spectroscopy of Poly4

4.2: Scanning Electron Microscopy Analysis of P3HT Films

In Figure(5 , 6 , 7 , 8) we present scanning electron microscopy (SEM) images of a heterojunction . These images provide a visual representation of the SEM measurements conducted on the sample. Notably, they reveal the presence of an intermediate layer within the heterojunction. This intermediate layer exhibits the formation of an interpenetrated network throughout the active layer film, resulting in a textured surface with uniformly distributed flake-like grains.

Upon closer examination, we conducted detailed analyses that yielded intriguing insights. In one instance, the variable range measured was less than 93.069 nanometers IN Poly4 .

As a significant outcome of our investigations, it was determined that the polymeric film formed on the nanoparticles in the samples ranged from 5.2 nanometers to 9.3 nanometers . This range of polymer layer thickness is crucial, as it classifies the layer as transparent, with the ability to transmit a substantial amount of light.

In summary, our SEM analysis not only provides a visual glimpse into the heterojunction structure but also offers valuable data on the thickness and characteristics of the polymer layer, which is instrumental in its light-transmitting properties.

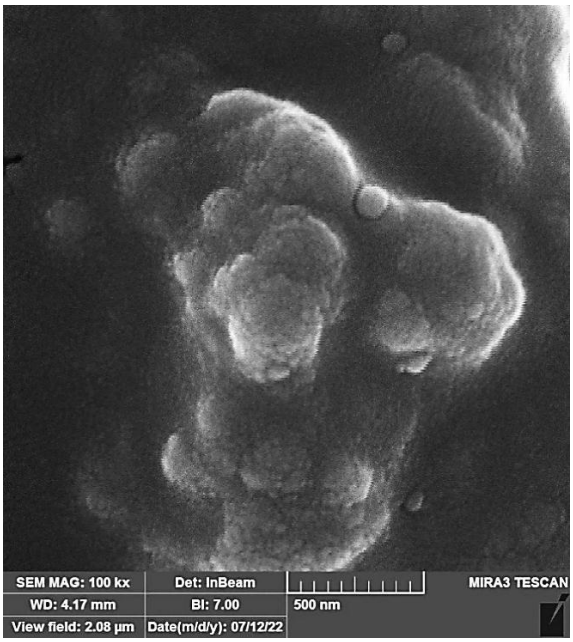

Figure (5) Scanning Electron Microscopy of Poly1

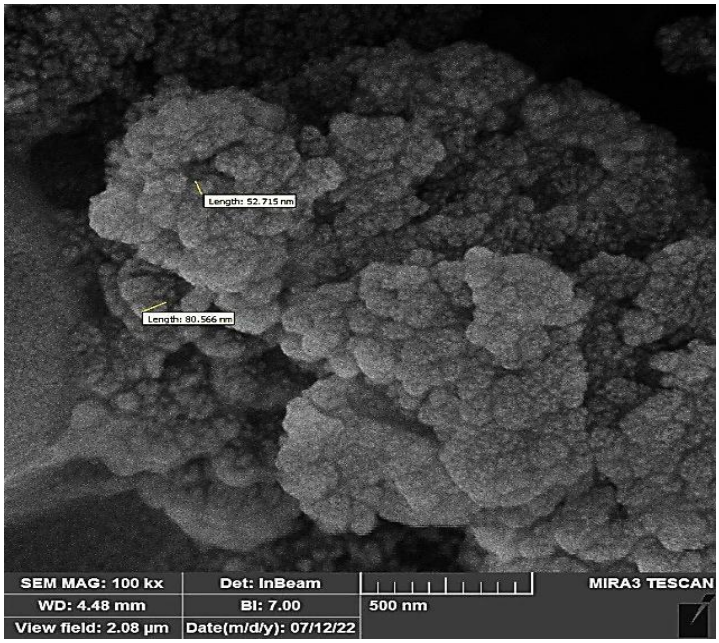

Figure (6) Scanning Electron Microscopy of Poly2

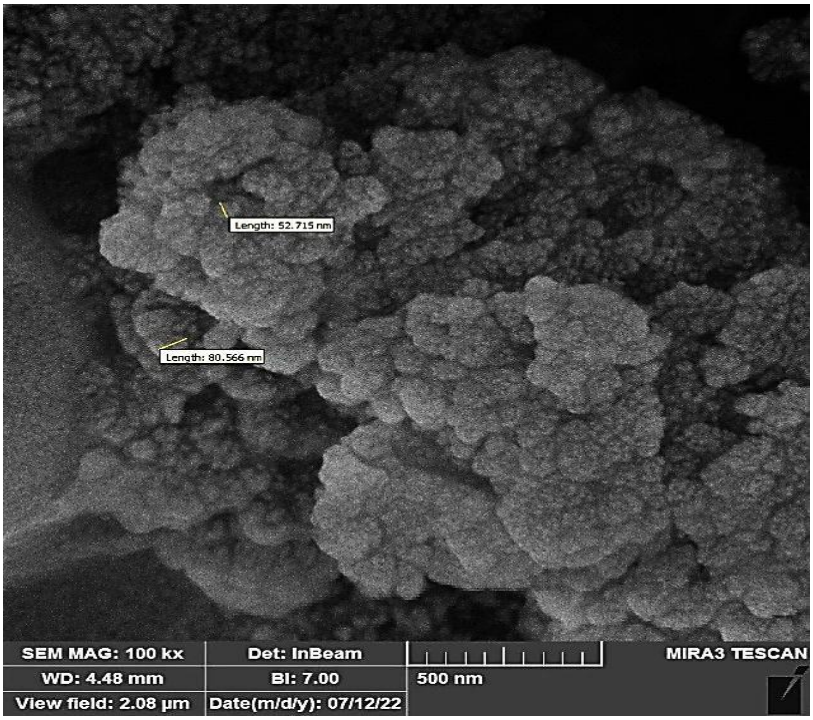

Figure (7) Scanning Electron Microscopy of Poly3

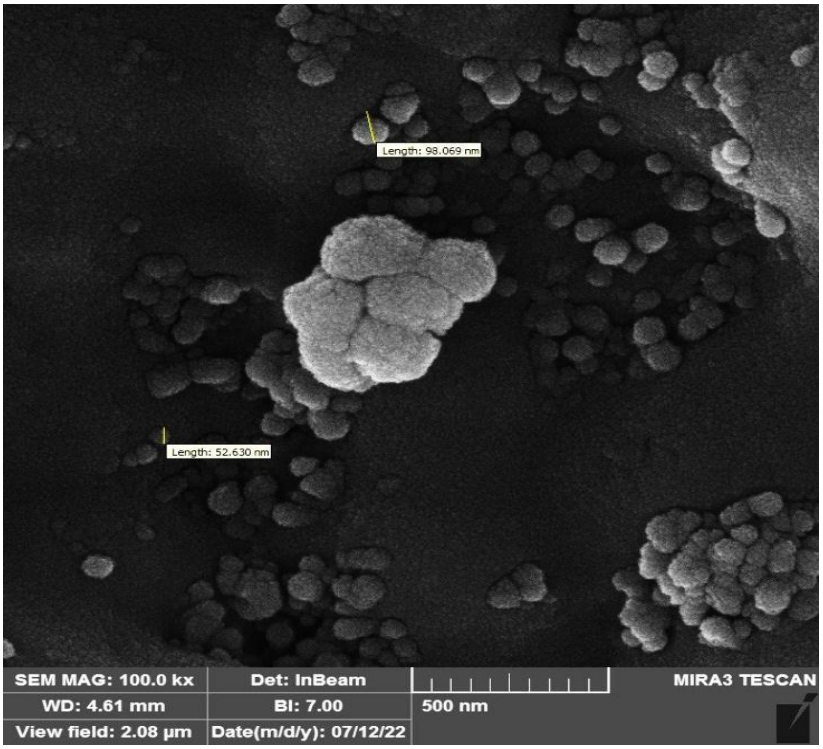

Figure (8) Scanning Electron Microscopy of Poly4

4.3: Atomic Force Microscopy (AFM) Analysis

We used the Atomic Force Microscopy device from University of Tehran, Iran (Newport Multimode™ Model 401).

To investigate the surface properties of Nano polymer membranes, these polymers were meticulously deposited onto silicon substrates. During the measurement process, the tip mode of an atomic force microscope (AFM) was employed.

The accompanying figures(from 9 to 12) show cases a sequence of images captured using AFM, each depicting a different dimension of the polymeric surfaces (10 nm). It's important to note that these measurements were conducted under standard environmental conditions.

The images reveal intriguing details. Notably, areas with a smaller cross-section exhibit more pronounced grain sizes. Furthermore, we observe the consistent formation of atomic structures and similar shape features across these polymeric surfaces. Additionally, clusters of atoms and molecules are discernible. These clusters may arise from variations in the binding energy of chemical bonds within the polymer structure.

Furthermore, the AFM imaging allows us to gain insights into the three-dimensional structure of the polymeric membrane, providing a thorough examination of its thickness, which measures approximately between 20.6 to 5.02 nanometers , It was compared with some published research[25].

In terms of surface roughness, the polymer film exhibits values ranging from 10.4 nanometers to 2.59 nanometers. It was compared with some published research[26 ,27].

AFM analysis unveils valuable information about the surface properties of Nano polymer membranes, including the distribution of grain sizes, the presence of atomic clusters, and the surface roughness , all of which contribute to a comprehensive understanding of the material's characteristics and potential applications.

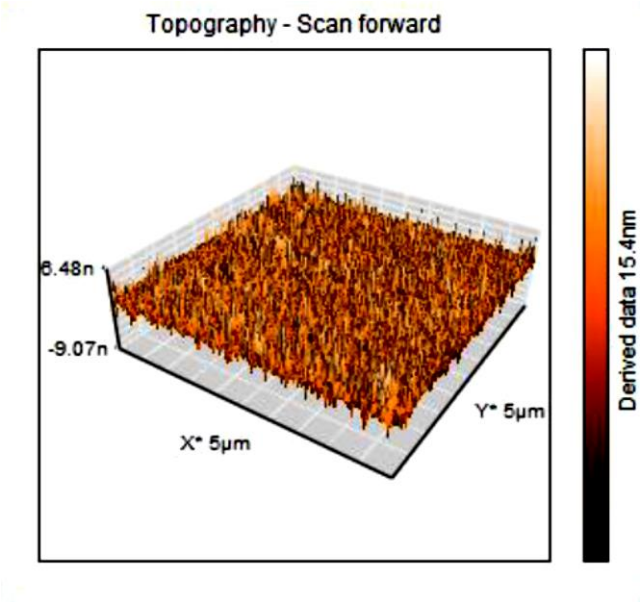

Figure (9) Atomic Force Microscopy of Poly1

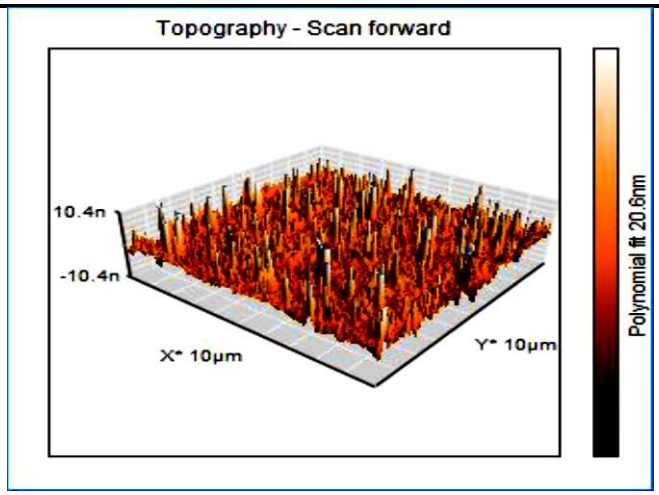

Figure (10) Atomic Force Microscopy of Poly2

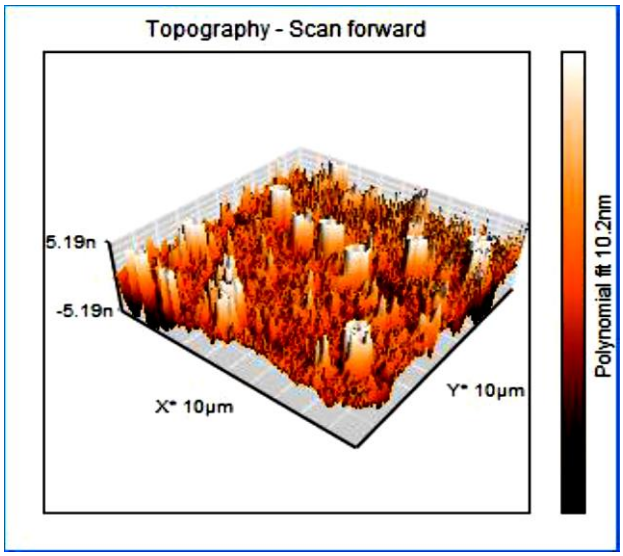

Figure (11) Atomic Force Microscopy of Poly3

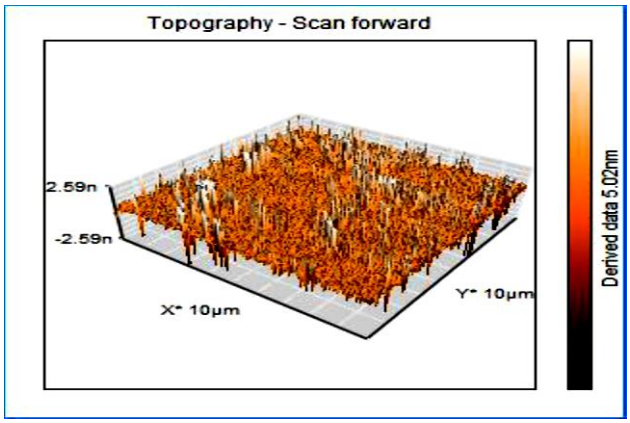

Figure (12) Atomic Force Microscopy of P Poly4

4.4: X-Ray Diffraction (XRD) Analysis

We used X-Ray Diffraction device from University of Tehran, Iran .

The study utilized X-ray diffraction (XRD) to examine material structures, fig (13 , 14 , and 15 ,16) FOR revealing several key insights.

Polymers, due to their low X-ray absorption, allow minimal interference, yet even highly crystalline ones contain amorphous regions owing to inherent structural irregularities.

Achieving a completely monocrystalline polymer structure is challenging due to these complexities. Broad XRD peaks indicate structural defects within polymers, while higher polymer crystallinity necessitates high viscosity and low permeability for a more ordered molecular arrangement. Specific XRD patterns of P3HT and Thiophene highlighted indicating crystallinity in P3HT and an amorphous structure in Thiophene. Quantitative peak data provided crucial insights into material crystalline properties, enabling the distinction between crystalline and amorphous phases and offering valuable information on material structural behaviors.

From the results of the X-ray analysis shown in the tables, the crystal lattice parameter was obtained, and these results are identical to the sources [28 , 29 , 30 , 31 , 32 ,33,34,35,36].

X-ray diffraction pattern of the formed nanoparticles is shown in Figure (13, 14 and 15,16).

A number of Bragg reflection peaks were observed at 2θ values of (13.85146) (15.15045) ,(16.74849) ,(18.50793),(19.20878),(21.81976),(19.73422),(24.75264),(24.9355), (25.09783),(28.0785),(32.3364),(38.62958),(42.68042),(44.84426),(46.39774),(54.95699), (57.58991),(65.2434),(67.72594),(74.73902),(76.99064),and (78.39391) which are indexed (002) ,(002),(003)) ,(401) ,(404),(404), (100), (211) ,(100), (123), (110), (231), (111), (200), (200) ,(142) ,(142),(241), (220), (200) ,(004), (311) and (311).

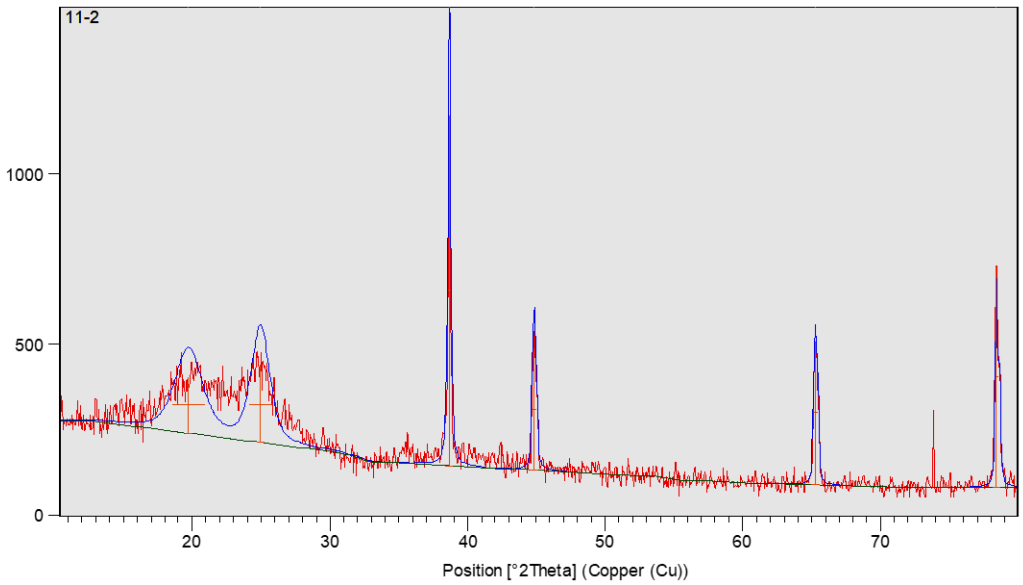

Figure (13) X-Ray Diffraction of Poly1

Table 2: X-ray diffraction data for **Poly**1

Pos. [°2Th.]	Height [cts]	FWHM [°2Th.]	d-spacing [Å]	Rel. Int. [%]	Tip Width
19.73422	165.3736	2.3616	4.49884	16.12	2.8339
24.93554	225.3268	1.5744	3.57096	21.96	1.8893
38.62958	1026.05	0.246	2.33082	100	0.2952
44.84426	359.1008	0.2952	2.02119	35	0.3542
65.2434	419.373	0.246	1.43007	40.87	0.2952
78.3939	647.5464	0.1968	1.21986	63.11	0.2362

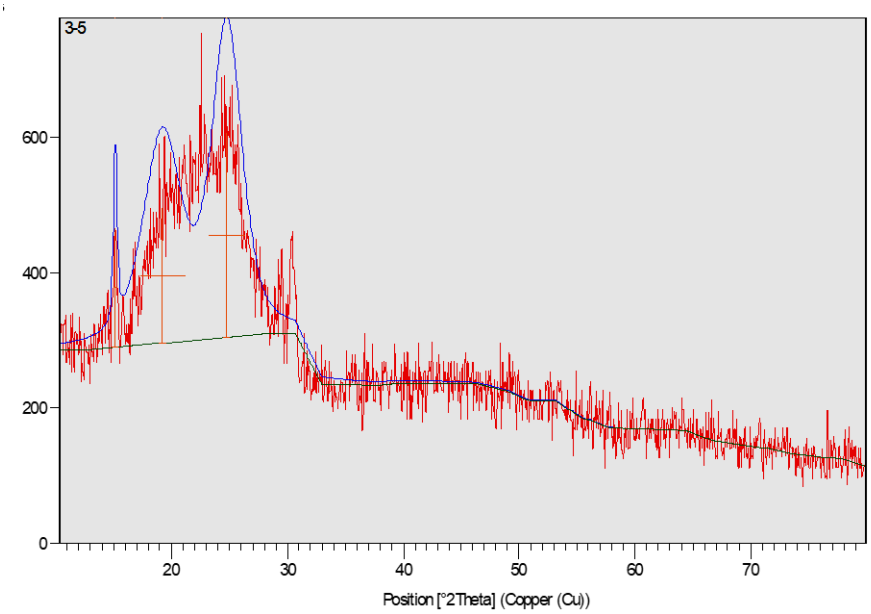

Figure (14) X-Ray Diffraction of Poly2

Table 3: X-ray diffraction data for **Poly**2

Pos. [°2Th.]	Height [cts]	FWHM [°2Th.]	d-spacing [Å]	Rel. Int. [%]	Tip Width
15.15045	176.9974	0.393600	5.84806	58.13	0.4723
19.20878	201.8192	3.936	4.6207	66.28	4.7232
24.75264	304.49	3.1488	3.59693	100	3.7786

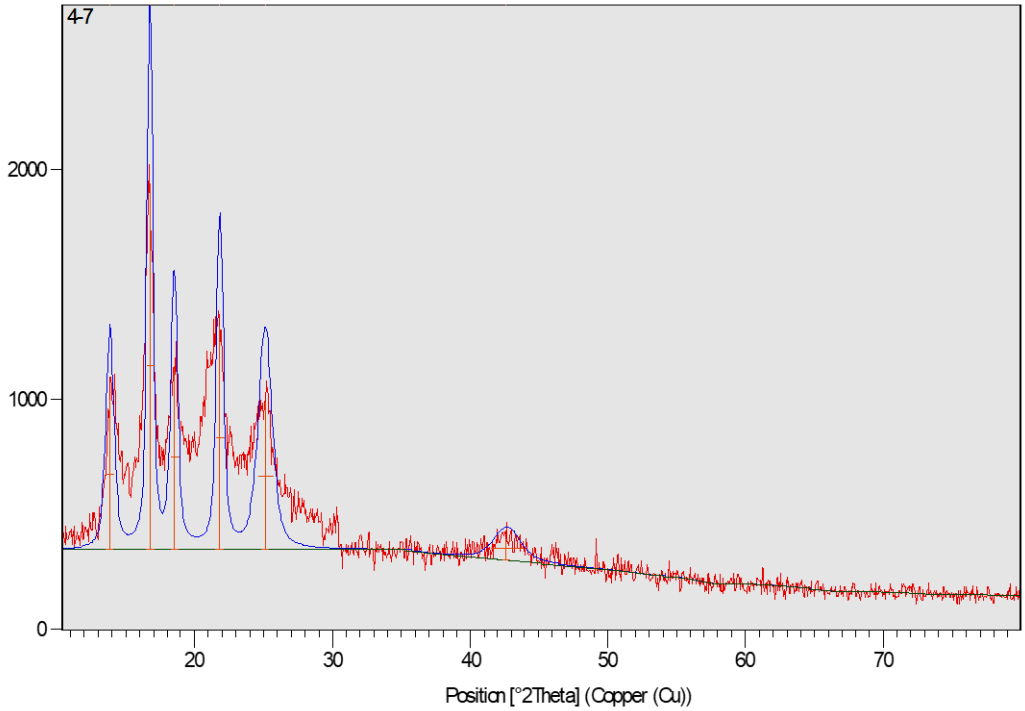

Figure (15) X-Ray Diffraction of Poly3

Table 4: X-ray diffraction data for **Poly**3

Pos. [°2Th.]	Height [cts]	FWHM [°2Th.]	d-spacing [Å]	Rel. Int. [%]	Tip Width
13.85146	656.3513	0.6888	6.39343	41.05	0.8266
16.74849	1598.862	0.492	5.2935	100	0.5904
18.50793	798.5269	0.5904	4.79406	49.94	0.7085
21.81976	975.8159	0.5904	4.07333	61.03	0.7085
25.09783	647.5964	1.1808	3.54824	40.5	1.417
42.68042	97.6615	2.3616	2.11851	6.11	2.8339

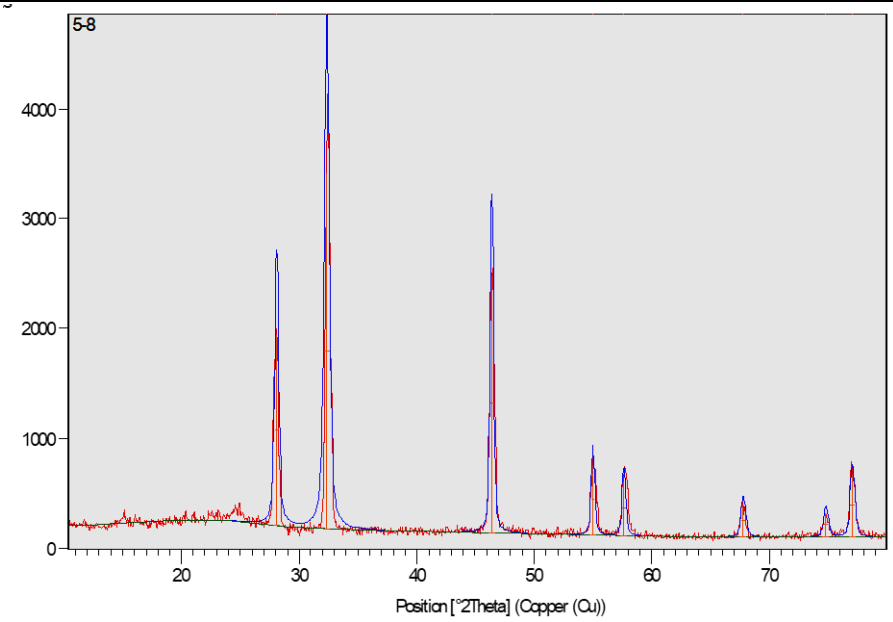

Figure (16) X-Ray Diffraction of Poly4

Table 5: X-ray diffraction data for **Poly**4

Pos. [°2Th.]	Height [cts]	FWHM [°2Th.]	d-spacing [Å]	Rel. Int. [%]	Tip Width
28.07855	1733.01	0.3936	3.17798	53.52	0.4723
32.33641	3238.062	0.492	2.76859	100	0.5904
46.39774	2350.948	0.2952	1.95707	72.6	0.3542
54.95699	636.0988	0.2952	1.67081	19.64	0.3542
57.58991	493.3281	0.2952	1.60053	15.24	0.3542
67.7259	288.7709	0.3936	1.38357	8.92	0.4723
74.73902	218.9237	0.3936	1.27018	6.76	0.4723
76.99064	564.489	0.3444	1.23855	17.43	0.4133

4.5: Optical Properties

We used UV device from University of Basra, College of Education for Pure Sciences, Department of Physics (shimadzu corporation Jaban , UV -1800 240V).

Copolymer films deposited onto glass substrate after annealing at 70 0C for 30 min in the wavelength between 200 - 800 nm.

the main absorption wavelength region of samples Poly1 , Poly2 , Poly3 , Poly4 is around λ~ 490nm . The UV- absorption spectra of the all films were plotted in Figure (17) featured absorption bands around λ~510, 460 , 470 and 500 nm , respectively.

The main peak at ~490 nm is attributed to the π–π* transition in crystalline π-π stacking structure of polymer P3HT chains (conjugated polymer)[37].The variation of absorbance with wavelength for samples Poly1 , Poly2 , Poly3 , Poly4 are shown in figure (17) . The figure

show peak appears at 510nm for Poly1 .From drawing the relationship between absorption coefficient and photon energy of Poly1 , Poly2 , Poly3 , Poly4.

The value of absorption coefficient plays an important role in the limitation of the type of transition. From the figure(17) the value of the (α)was greater than (10^4 cm-1) indicating that the transition was direct electron transmission.

The figs (from 18 to 21) provided illustrates the relationship between (hν) versus (hνα)^2 and the photon energy of the samples.

The energy gap was determined by identifying the intersection point of the linear relationship with hν yielding values of approximately) 2 eV , 2.07 eV , 2.05 eV for samples Poly2 , Poly3 , Poly4 respectively) , While copolymers Poly1 without nanoparticles had greater The energy gap (2.3eV) .

Table 6: presents the energy gap values for the various samples. Notably, a discernible trend emerges from the figures: the energy gap diminishes as nanoparticles are introduced, decreasing from(2.3 eV) to (2.05 eV). This signifies a reduction in the energy gap by 0.19 eV following doping.

The decrease in the energy gap can be elucidated by the heightened concentration of nanoparticles. As doping levels increase, there is an augmentation in the number of polar on states introduced within the energy gap, ultimately leading to its contraction[38].

Moreover, the increase in the absorption coefficient observed with increasing nanoparticle concentration can be attributed to the absorption of additional photons by the newly generated energy levels within the gap. These levels multiply in number as doping levels rise, contributing to the augmented absorption coefficients[39].

The analysis of optical properties, specifically the energy gap and absorption coefficients, provides valuable insights into the impact of nanoparticle doping on the material's electronic structure, shedding light on its potential applications in optoelectronic devices[40].

The refractive index dispersion can be analyzed by the single-oscillator model [41].

$$n^2 + 1 = \frac{E_d + E_o}{{E_o}^2 - (h\nu)^2} \dots\dots\dots (5)$$

Where n is the refractive index, h is Planck's constant, ν is the frequency,(hν) is the photon energy, E_o is the average excitation energy for electronic transitions, and E_d is the dispersion energy which is a measure of the strength of interband optical transitions. From the drawing between $(\frac{1}{n^2-1})$ versus $(h\nu)^2$ Fig(from 22 to 25).The oscillator parameters

E_o and E_d values were determined from the slope $(E_o\ E_d)^{-1}$ and the intercept (E_0/E_d) on the vertical axis respectively.

From there it was determined the values of the oscillator parameters (E_o, and E_d) The oscillator energy, E_o is related to the optical band gap tabulated in table (6). It is known that inter-material boundaries contain structural defects and impurities. These factors have a strong influence on the absorption processes [42].

The long wavelength refractive index ($\mathbf{n}_\infty$) and average oscillator wave

length (λ_o) and oscillator length strength S_o can be estimated by the single oscillator model givenby [43].

$$\frac{n_\infty^2 - 1}{n^2 - 1} = 1 - \frac{\lambda_o^2}{\lambda^2} \quad \ldots.(6\ )$$

The value of (n_∞) was calculated from the line segments between ($\frac{1}{n^2-1}$) and ($\frac{1}{\lambda^2}$) shown in the figures (from 26 to 29).from the curve plotted are given in table (6). Eq. (6) become:-

$$\boldsymbol{n^2 - 1 = \frac{s_o \lambda^2}{1 - \frac{\lambda_o^2}{\lambda^2}}} \quad \boldsymbol{\ldots\ldots\ldots\ldots(7)}$$

where $S_0 = (n_\infty - 1)/\lambda^2$ is the average oscillator parameter which is the strength of the individual dipole oscillator. The So value was estimated using Eq. above and are given in table (6).

The M-1 and M-2 moments of the optical spectra are expressed as [44].

$$E_o^2 = \frac{M_{-1}}{M_{-3}} \ , E_d^2 = \frac{M_{-1}^3}{M_{-1}} \quad \ldots\ldots\ldots\ldots (8)$$

The M-1, M-3 moments were estimated using the above equation and are given in table (6). The M-1, and M-2 moments changed due to the formation coordination of complex. The third order nonlinear susceptibility (χ 3) has been calculated from the following equation (8) and tabulated in table (6).

$$X^3 = A\left[\left(\frac{E_o E_d}{4\pi(E_o^2 - (h\nu)^2}\right)^4\right] = \frac{\mathbf{A}}{(\mathbf{4\pi})^4\ (\boldsymbol{n^2 - 1})^4} \ldots\ldots\ldots(9)$$

The provided table encapsulates essential optical properties of diverse materials and compositions at distinct wavelengths and energy levels. Each entry delineates parameters crucial in understanding the materials' response to light, encompassing nonlinear optical behavior (Third-order visual effect X^3 , The Average Oscillator S_o) , energy-related characteristics (Moments Of The Optical Spectra For Liquid Crystal M-3 , Moments Of The Optical Spectra For Liquid Crystal M-1, and key optical traits (refractive index, energy dissipation, band gap energy). For instance, P3HT showcases moderate values across parameters, indicating its potential in specific electronic applications with a band gap energy (Eg) of 2.3 eV FOR Poly1 . Furthermore, the compositions blending P3HT with varying nanoparticles (SiO_2 NP, ZnO NP, Ag NP) exhibit distinctive properties, showcasing sensitivity to compositional changes. These findings suggest potential applications in optoelectronics and photonics, implying materials with specific band gap energies may suit distinct uses like solar cells or light-emitting devices. However, further analysis and experimentation are warranted to unravel the full implications and applications of these materials based on their intricate optical properties[45].

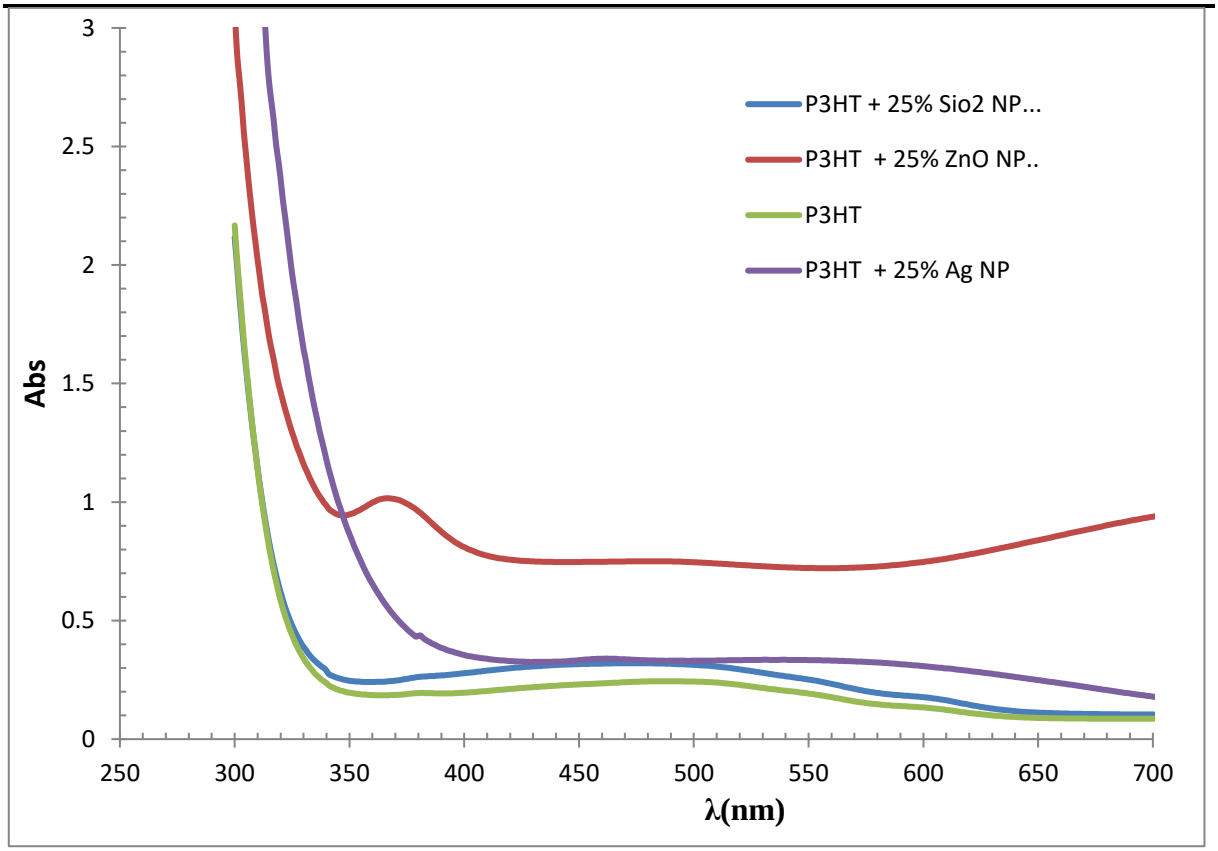

Figure (17) absorption of Poly1 , Poly2 , Poly3 , Poly4

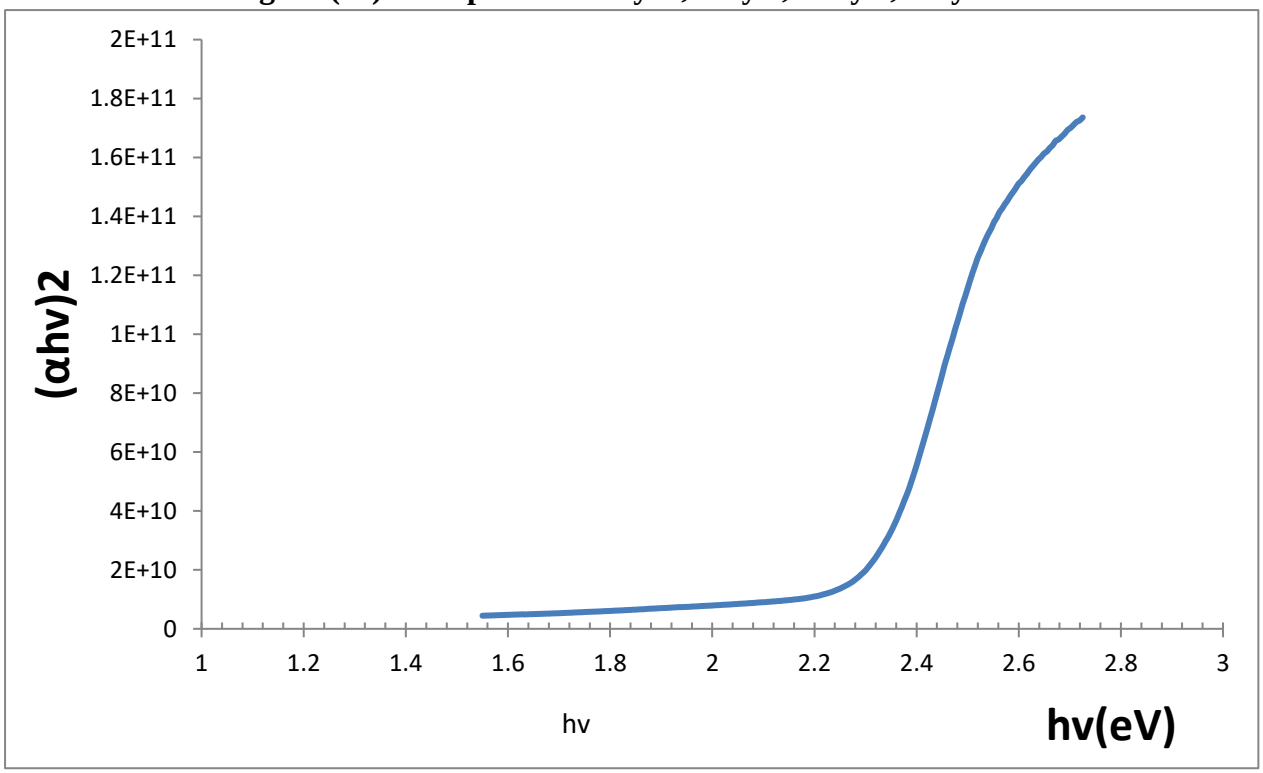

Figure (18) Band gab Energy of Poly1

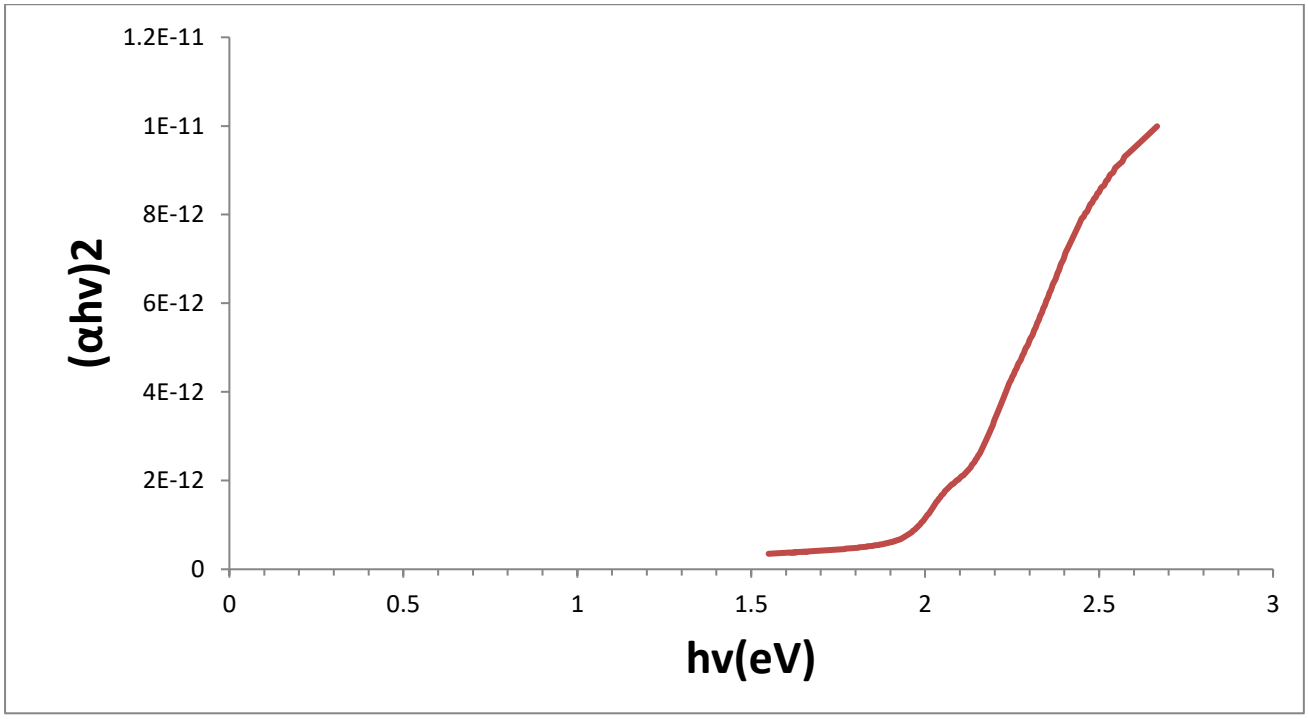

Figure (19) Band gab Energy of Poly2

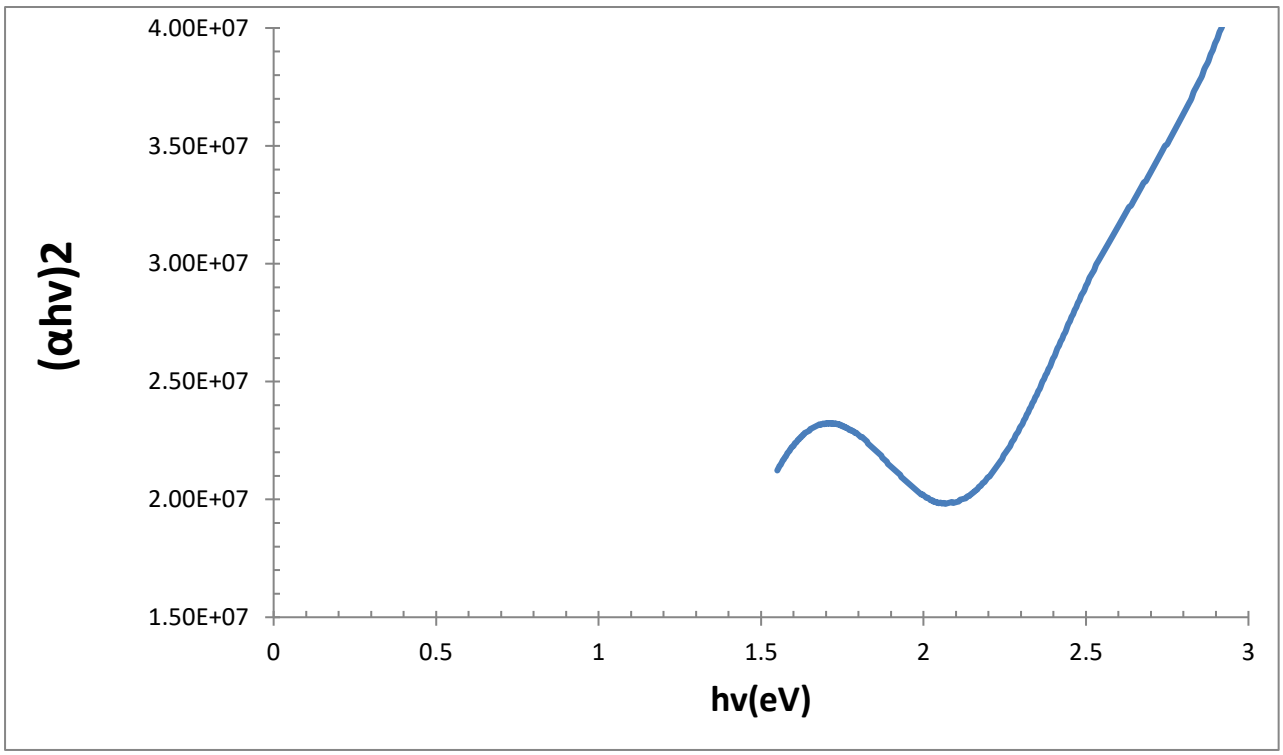

Figure (20) Band gab Energy of Poly3

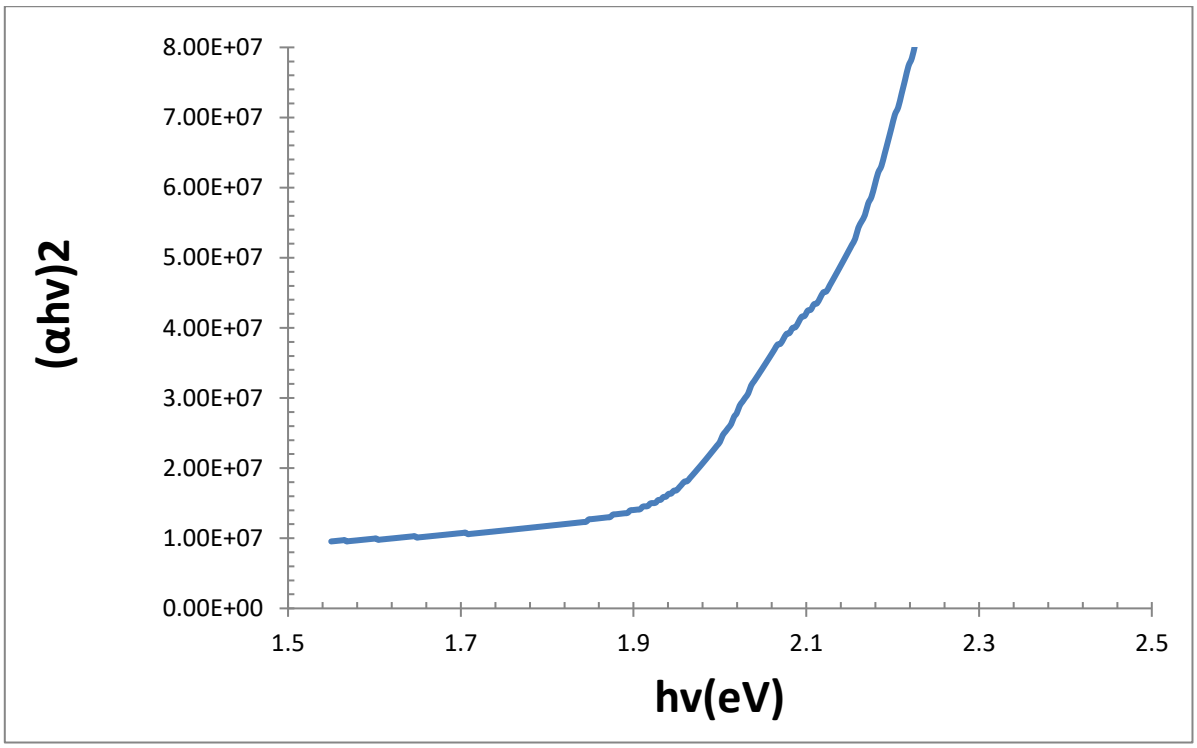

Figure (21) Band gab Energy of Poly4

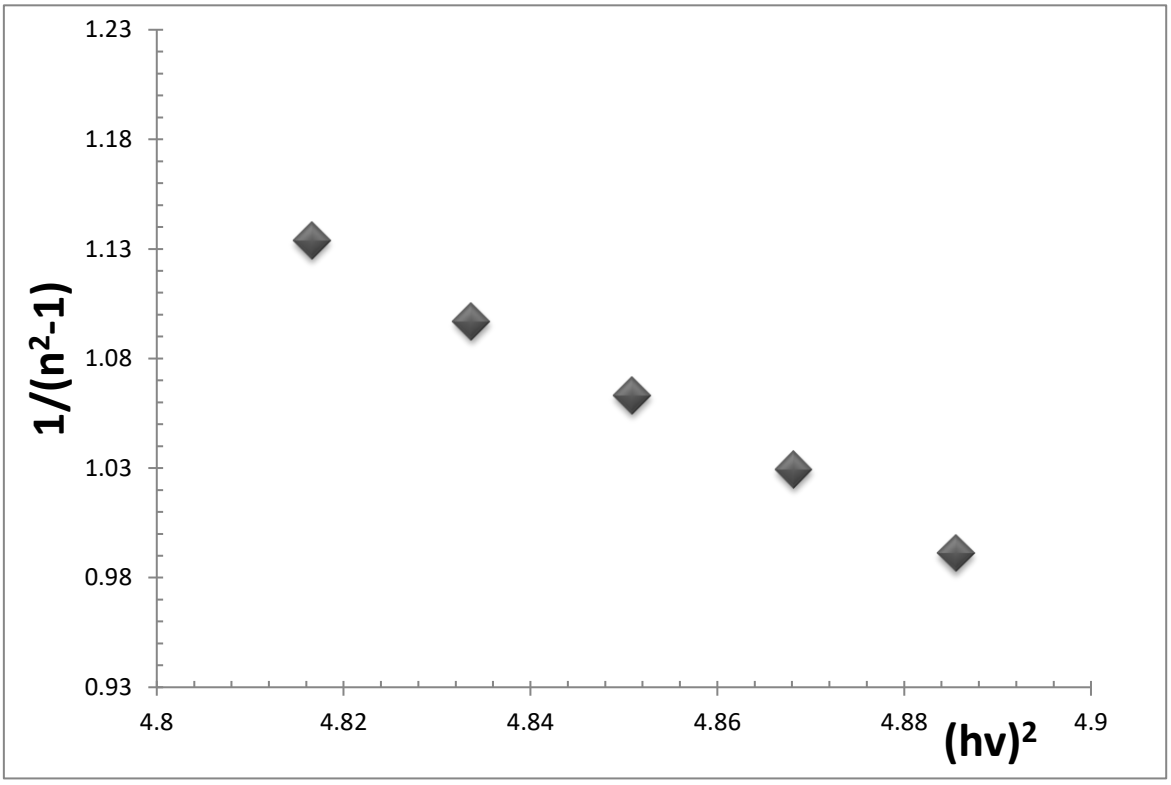

Figure (22) relationship between ($\frac{1}{n^2-1}$) versus $(hv)^2$ of Poly1 .

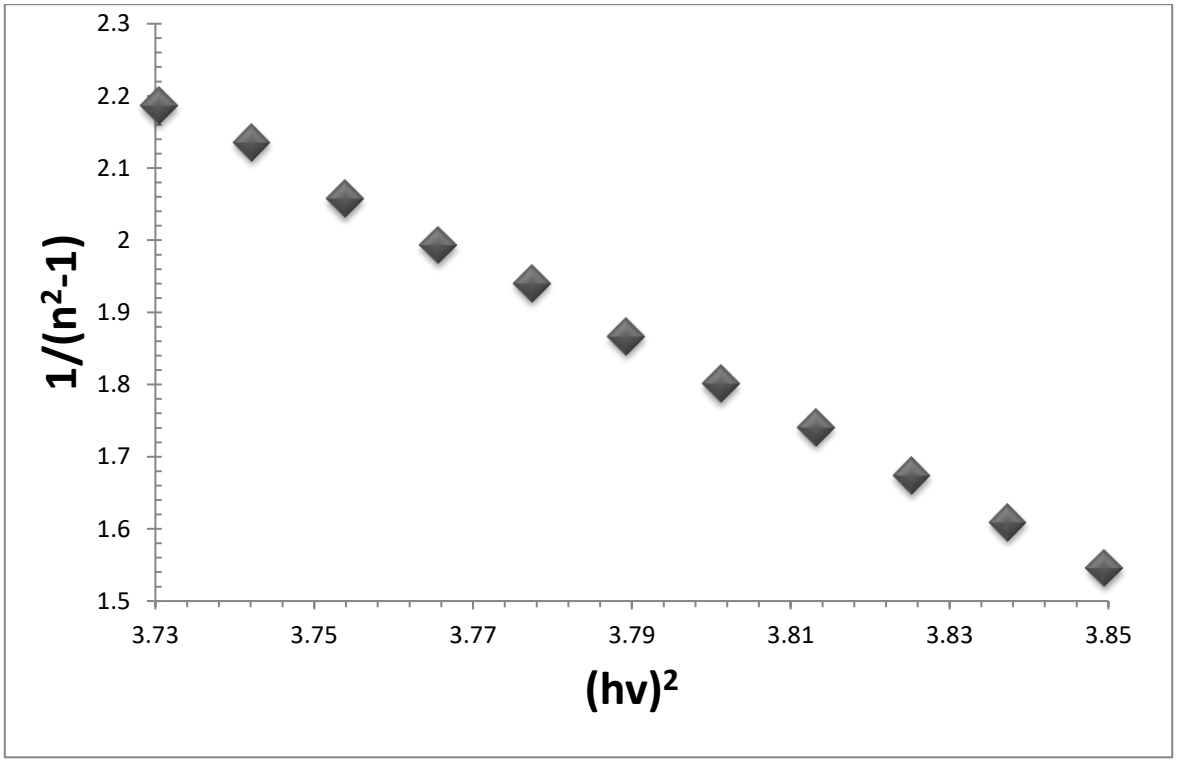

Figure (23) relationship between ($\frac{1}{n^2-1}$) versus $(h\nu)^2$ of Poly2 .

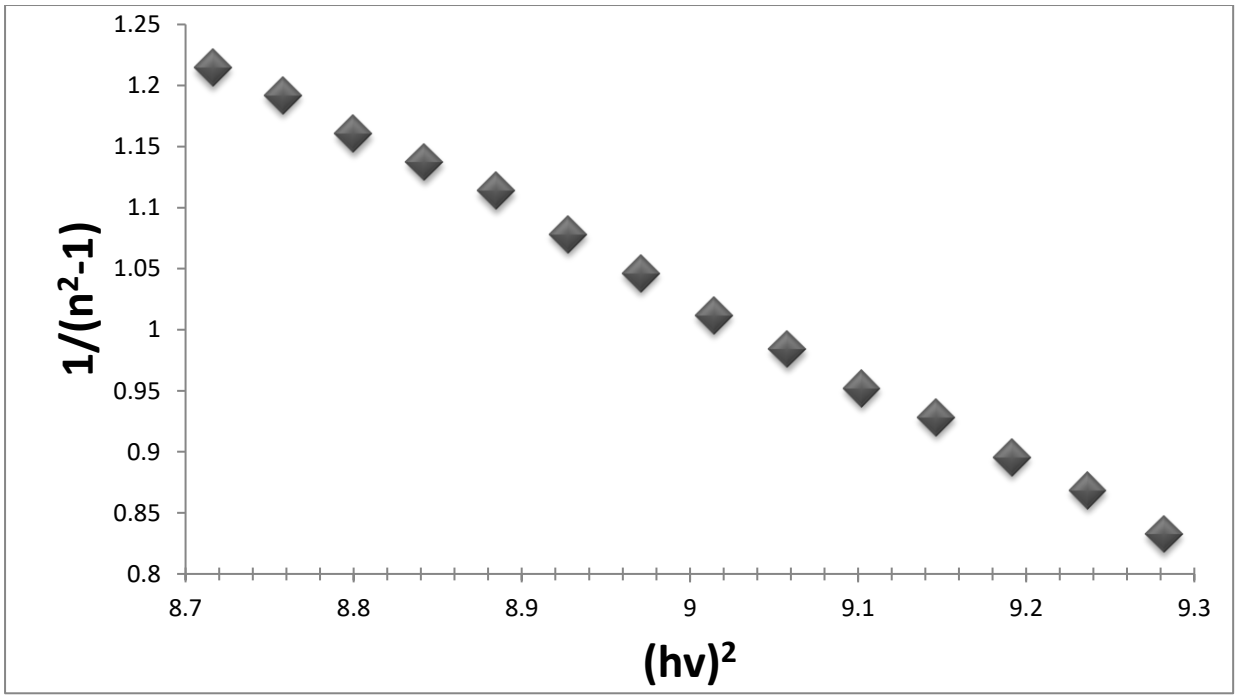

Figure (24) relationship between ($\frac{1}{n^2-1}$) versus $(h\nu)^2$ of Co-Poly3.

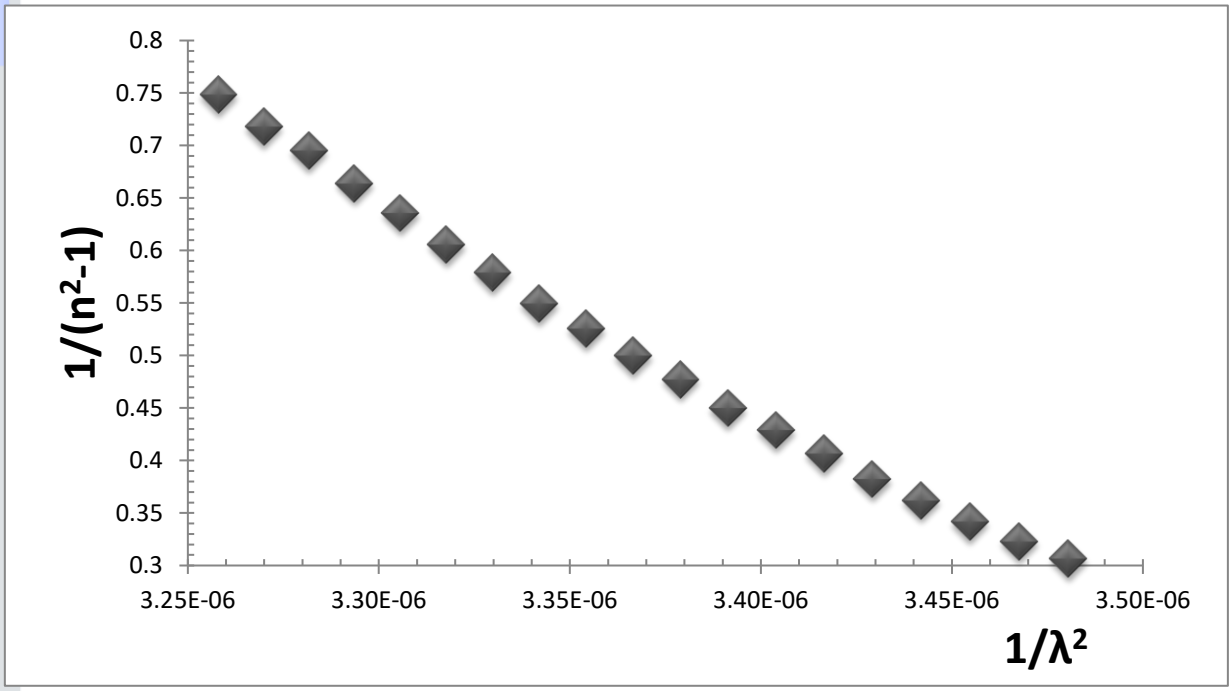

Figure (25) relationship between ($\frac{1}{n^2-1}$) versus $(hv)^2$ of Co-Poly4.

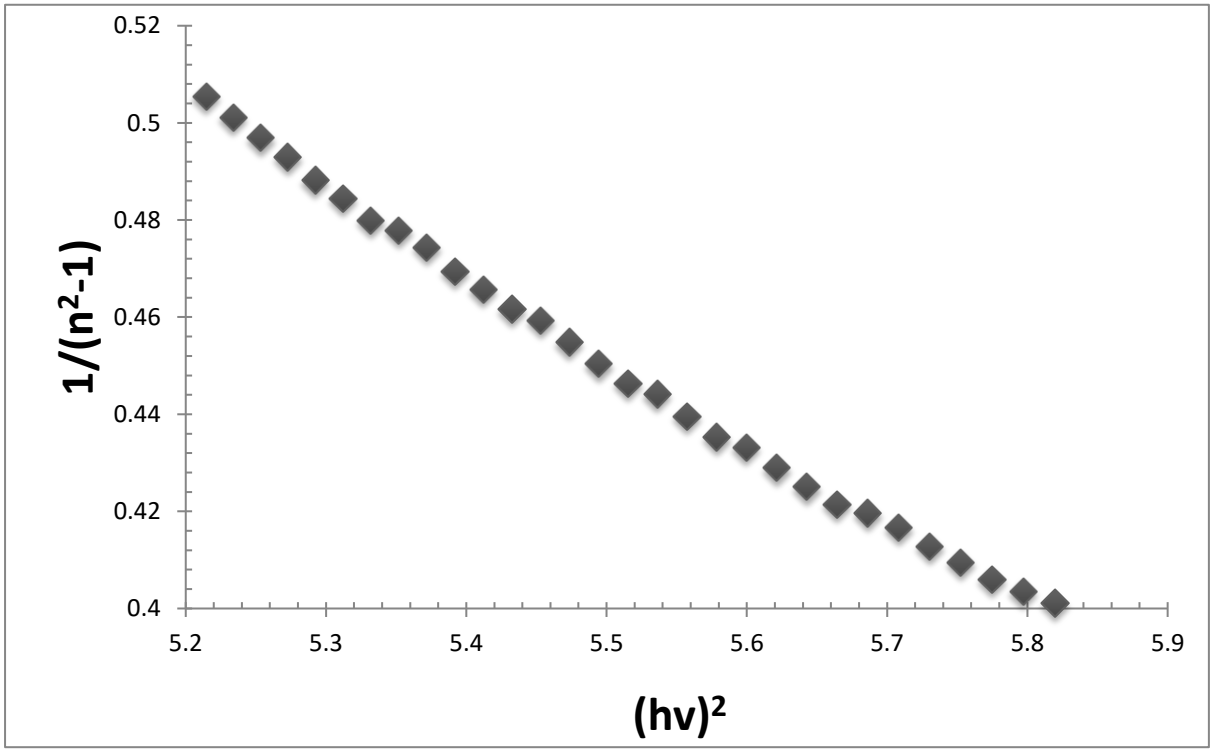

Figure (26) relationship between ($\frac{1}{n^2-1}$) versus ($\frac{1}{\lambda^2}$) of Poly1 .

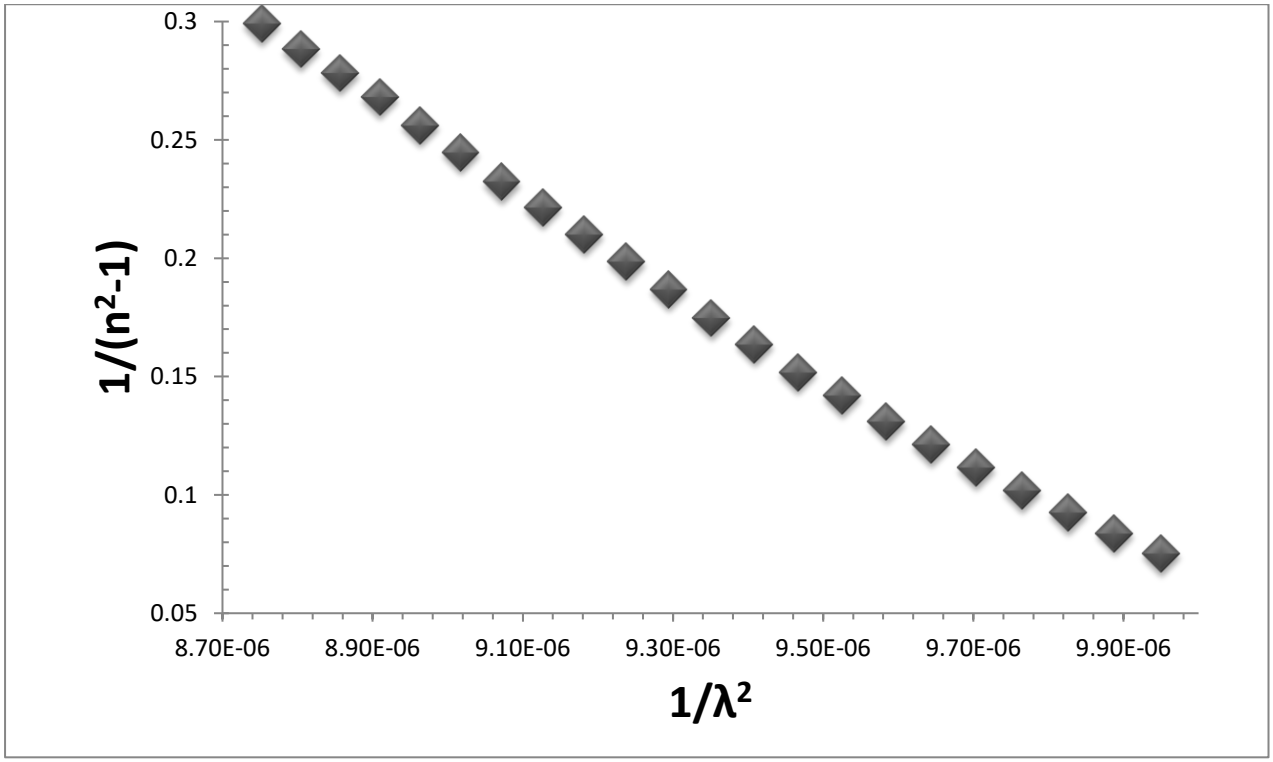

Figure (27) relationship between ($\frac{1}{n^2-1}$) versus ($\frac{1}{\lambda^2}$) of Poly2 .

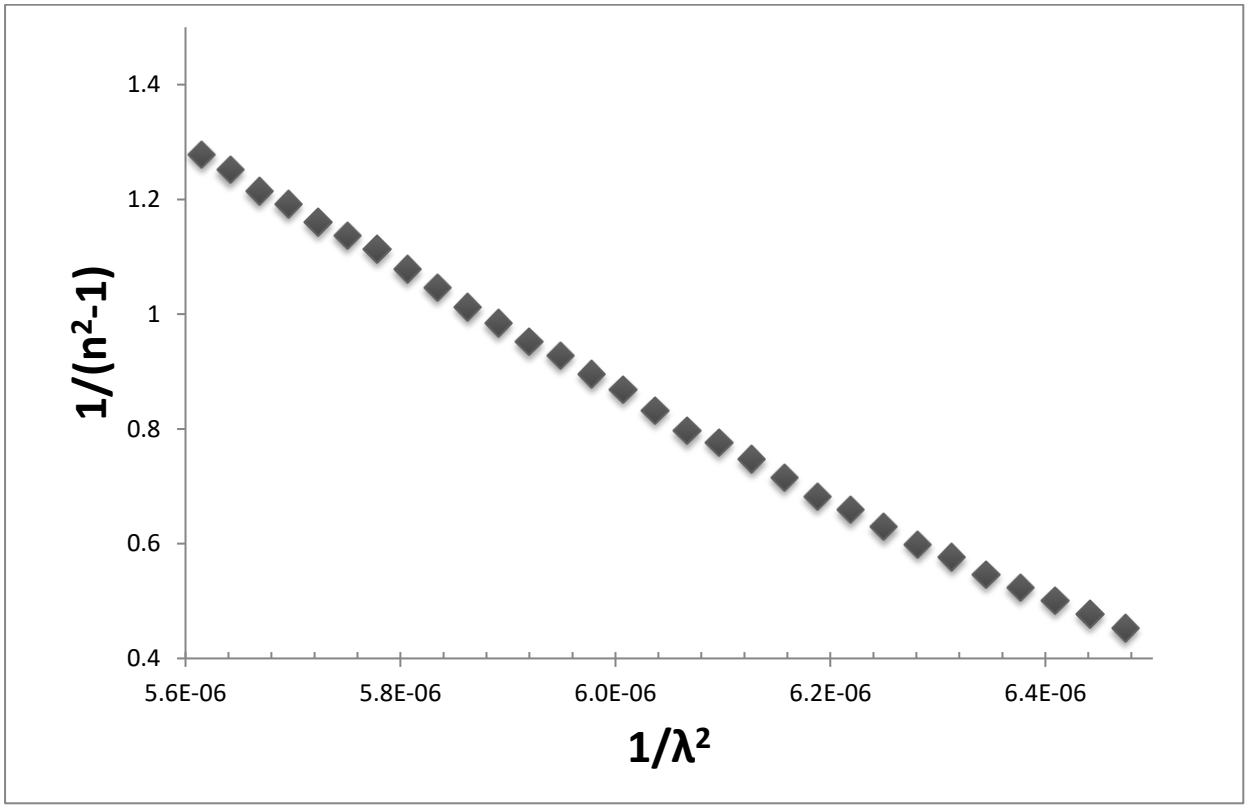

Figure (28) relationship between ($\frac{1}{n^2-1}$) versus ($\frac{1}{\lambda^2}$) of Co-Poly3.

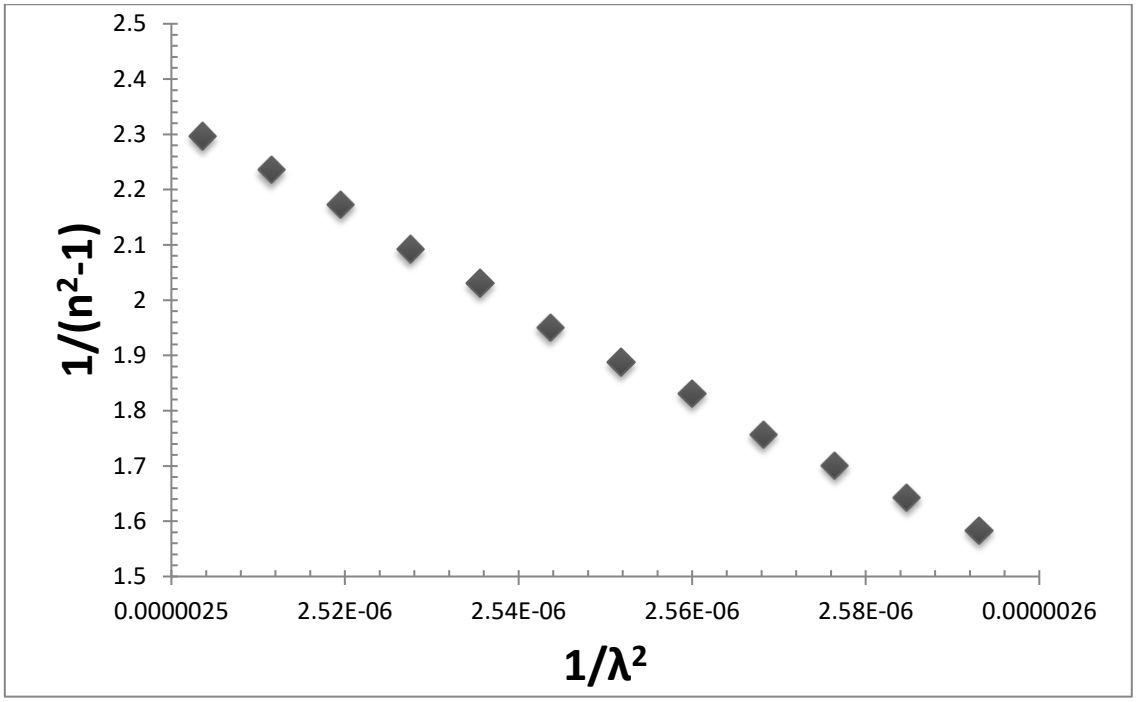

Figure (29) relationship between ($\frac{1}{n^2-1}$) versus ($\frac{1}{\lambda^2}$) of Co-Poly4.

Table 6: (parameters some optical properties)

sample	Poly1	Poly2	Poly3	Poly4
E_g (eV)	2.3	2	2.07	2.05
E_0 (ev)	2.175	1.0325	1.428	1.471
E_d(eV)	0.435	0.149	1.0988	0.086
n_o^2	1.4	1.0697	1.33	1.1267
ε_∞	1.0954	5.132	1.625	1.26
M-1	0.2	0.1353	0.377	0.0268
M-3	0.0423	0.1443	0.769	0.051
So	3.84 E-7	47.9E-7	10.87 E-7	13.25 E-7
X^3	1.078 E-24	9.6 E-24	2.04 E-24	7.52 E-24
λ_o(nm)	1095.94	928.43	758.287	442.93

5 :Conclusion

The study delves into enhancing polymer solar cells by incorporating hexylthiophene@NP (SiO_2, ZnO, Ag) into active layers, exploring their optical properties. Analyses using XRD, SEM, FTIR, AFM, and UV-visible absorption spectroscopy revealed crystallinity in nanoparticles, varying film thicknesses, and nanoparticle-polymer interactions. Results suggest potential applications in optoelectronics. The findings emphasize the promising role of these nanoparticles in improving the efficiency of polymer solar cells, hinting at their prospective industrial utility in solar energy conversion systems.

References

1) Ansari, Muhammad Azhar, et al. "Synthesis and characterization of poly (3-hexylthiophene): improvement of regioregularity and energy band gap." *RSC advances* 8.15 (2018): 8319-8328.

2) Liu, J., Yao, M., & Shen, L. (2019). Third generation photovoltaic cells based on photonic crystals. *Journal of Materials Chemistry C*, *7*(11), 3121-314

3) Wang, Ziying, et al. "Recent advances in natural functional biopolymers and their applications of electronic skins and flexible strain sensors." *Polymers* 13.5 (2021): 813.

4) Cui, Chen, et al. "Recent progress in natural biopolymers conductive hydrogels for flexible wearable sensors and energy devices: materials, structures, and performance." *ACS applied bio materials* 4.1 (2020): 85-121.

5) Le, Thanh-Hai, Yukyung Kim, and Hyeonseok Yoon. "Electrical and electrochemical properties of conducting polymers." *Polymers* 9.4 (2017): 150.

6) Das, Pankaj Kumar, and Anuj Dhawan. "Plasmonic enhancement of photovoltaic characteristics of organic solar cells by employing parabola nanostructures at the back of the solar cell." *RSC advances* 13.38 (2023): 26780-26792.

7) Urien, Mathieu, et al. "Effect of the regioregularity of poly (3-hexylthiophene) on the performances of organic photovoltaic devices." *Polymer international* 57.5 (2008): 764-769.

8) Arias, Jose Jonathan Rubio, and Maria de Fatima Vieira Marques. "Performance of poly (3-hexylthiophene) in bulk heterojunction solar cells: Influence of polymer size and size distribution." *Reactive and Functional Polymers* 113 (2017): 58-69.

9) Subramanyam, B. V. R. S., et al. "Investigation of improvement in stability and power conversion efficiency of organic solar cells fabricated by incorporating carbon nanostructures in device architecture." *Journal of Physics: Materials* 3.4 (2020): 045004.

10) Printz, Adam D., and Darren J. Lipomi. "Competition between deformability and charge transport in semiconducting polymers for flexible and stretchable electronics." *Applied Physics Reviews* 3.2 (2016).

11) Wang, Ging-Ji Nathan, Andrea Gasperini, and Zhenan Bao. "Stretchable polymer semiconductors for plastic electronics." *Advanced Electronic Materials* 4.2 (2018): 1700429.

12) Chaudhary, Vivek, et al. "Highly aligned and crystalline poly (3-hexylthiophene) thin films by off-center spin coating for high performance organic field-effect transistors." *Synthetic Metals* 258 (2019): 116221.

13) Kim, Nam-Koo, et al. "High-performance organic field-effect transistors with directionally aligned conjugated polymer film deposited from pre-aggregated solution." *Chemistry of Materials* 27.24 (2015): 8345-8353.
14) Jung, Sokhee P., and Soumya Pandit. "Important factors influencing microbial fuel cell performance." *Microbial electrochemical technology*. Elsevier, 2019. 377-406.
15) Liang, Junhao, Xing Ouyang, and Yan Cao. "Interfacial and confined molecular-assembly of poly (3-hexylthiophene) and its application in organic electronic devices." *Science and Technology of Advanced Materials* 23.1 (2022): 619-632.
16) Liang, Junhao, Xing Ouyang, and Yan Cao. "Interfacial and confined molecular-assembly of poly (3-hexylthiophene) and its application in." *Science and Technology of Advanced Materials*.
17) Chu, Ping-Hsun, et al. "Synergistic Effect of Regioregular and Regiorandom Poly (3-hexylthiophene) Blends for High Performance Flexible Organic Field Effect Transistors." *Advanced Electronic Materials* 2.2 (2016): 1500384.
18) Qiu, Guo, et al. "Niobium phosphotungstates: excellent solid acid catalysts for the dehydration of fructose to 5-hydroxymethylfurfural under mild conditions." *RSC advances* 8.57 (2018): 32423-32433.
19) Sharma, Shyamalima. "Development of polymer nanocomposite based photovoltaic devices with improved efficiency." (2016).
20) Zahn, Dietrich RT, Gianina N. Gavrila, and Georgeta Salvan. "Electronic and vibrational spectroscopies applied to organic/inorganic interfaces." *Chemical reviews* 107.4 (2007): 1161-1232.
21) Šebek, Jiří, et al. "Spectroscopy of the C–H stretching vibrational band in selected organic molecules." *The Journal of Physical Chemistry A* 117.32 (2013): 7442-7452.
22) Steven, Soen, Elvi Restiawaty, and Yazid Bindar. "Routes for energy and bio-silica production from rice husk: A comprehensive review and emerging prospect." *Renewable and Sustainable Energy Reviews* 149 (2021): 111329.
23) Pawar, Omkar, et al. "Green synthesis of silver nanoparticles from purple acid phosphatase apoenzyme isolated from a new source Limonia acidissima." *Journal of Experimental Nanoscience* 11.1 (2016): 28-37.
24) Jaffri, Shaan Bibi, and Khuram Shahzad Ahmad. "Phytofunctionalized silver nanoparticles: green biomaterial for biomedical and environmental applications." *Reviews in Inorganic Chemistry* 38.3 (2018): 127-149.
25) N'Konou, Kekeli, et al. "Impact of Ag@ SiO2 core-shell nanoparticles on the photoelectric current of plasmonic inverted organic solar cells." *Synthetic Metals* 239 (2018): 22-28.
26) Alharbi, Nada, et al. "Quantitative nano-mechanical mapping AFM-based method for elastic modulus and surface roughness measurements of model polymer infiltrated ceramics." *Dental Materials* 38.6 (2022): 935-945.

27) Maryamnegari, Simin Moradi, Mohammad Reza Nateghi, and Razieh Mohebat. "Effect of sintering and infiltration conditions on nanoscale dual network SiO2/polymethyl metacrylate composites mimicking human enamel." *Journal of Dentistry* 126 (2022): 104311.

28) Priyadharshini, R.I.; Prasannaraj, G.; Geetha, N.; Venkatachalam, P. Microwave-mediated extracellular synthesis of metallic silver and zinc oxide nanoparticles using macro-algae (Gracilaria edulis) extracts and its anticancer activity against human PC3 cell lines. Appl. Biochem. Biotechnol. 2014, 174, 2777–2790.

29) Roy, K.; Sarkar, C.K.; Ghosh, C.K. Green snthesis of silver nanoparticles using fruit extract of Malus domestica and study of its antimicrobial activity. Dig. J. Nanomater. Biostruct. 2014, 9, 1137–1147.

30) Zak, A. Khorsand, et al. "X-ray analysis of ZnO nanoparticles by Williamson–Hall and size–strain plot methods." *Solid State Sciences* 13.1 (2011): 251-256.

31) Nandanwar, Ruchi, Purnima Singh, and Fozia Z. Haque. "Synthesis and characterization of SiO2 nanoparticles by sol-gel process and its degradation of methylene blue." *Am. Chem. Sci. J* 5.1 (2015): 1-10.

32) Ercan, Ender, et al. "Multilevel photonic transistor memory devices based on 1D electrospun semiconducting polymer/perovskite composite nanofibers." *Advanced Materials Technologies* 6.8 (2021): 2100080.

33) Meng, Yongde. "A sustainable approach to fabricating Ag nanoparticles/PVA hybrid nanofiber and its catalytic activity." *Nanomaterials* 5.2 (2015): 1124-1135.

34) Glusker, Jenny Pickworth, and Kenneth N. Trueblood. *Crystal structure analysis: a primer*. Vol. 14. Oxford University Press, 2010.

35) Jendrzejewska, Izabela, et al. "The Usefulness of X-ray Diffraction and Thermal Analysis to Study Dietary Supplements Containing Iron." *Molecules* 27.1 (2021): 197.

36) Saini, B. S., and Raminder Kaur. "X-ray diffraction." *Handbook of Modern Coating Technologies*. Elsevier, 2021. 85-141.

37) Chu, Ping-Hsun, et al. "Toward precision control of nanofiber orientation in conjugated polymer thin films: Impact on charge transport." *Chemistry of Materials* 28.24 (2016): 9099-9109.

38) Baylan, Elif, and Ozlem Altintas Yildirim. "Highly efficient photocatalytic activity of stable manganese-doped zinc oxide (Mn: ZnO) nanofibers via electrospinning method." *Materials Science in Semiconductor Processing* 103 (2019): 104621.

39) Mazumder, Julaiba Tahsina, et al. "First principle study on structural and optoelectronic properties and band-gap modulation in germanium incorporated tin (IV) oxide." *Materials Today Communications* 27 (2021): 102393.

40) Kumbhakar, Partha, Chinmayee Chowde Gowda, and Chandra Sekhar Tiwary. "Advance optical properties and emerging applications of 2D materials." *Frontiers in Materials* 8 (2021): 721514.

41) Ashery, A., A. A. M. Farag, and M. A. Shenashen. "Optical absorption and dispersion analysis based on single-oscillator model of polypyrrole (PPy) thin film." *Synthetic metals* 162.15-16 (2012): 1357-1363.

42) Badran, Hussain A., Hussain F. Hussain, and Khalid I. Ajeel. "Nonlinear characterization of conducting polymer and electrical study for application as solar cells and its antibacterial activity." *Optik* 127.13 (2016): 5301-5309.

43) Yakuphanoglu, F., A. Cukurovali, and I. Yilmaz. "Single-oscillator model and determination of optical constants of some optical thin film materials." *Physica B: Condensed Matter* 353.3-4 (2004): 210-216.

44) Yakuphanoglu, F., A. Cukurovali, and I. Yilmaz. "Determination and analysis of the dispersive optical constants of some organic thin films." *Physica B: Condensed Matter* 351.1-2 (2004): 53-58.

45) Akinwande, Deji, et al. "A review on mechanics and mechanical properties of 2D materials—Graphene and beyond." *Extreme Mechanics Letters* 13 (2017): 42-77.